



HHS Public Access

Author manuscript

Nat Neurosci. Author manuscript; available in PMC 2014 September 01.

Published in final edited form as:

Nat Neurosci. 2014 March ; 17(3): 367–376. doi:10.1038/nn.3636.

LRRK2 regulates synaptogenesis and dopamine receptor activation through modulation of PKA activity

Loukia Parisiadou^{1,2,5,6}, Jia Yu^{1,3,5}, Carmelo Sgobio^{1,5}, Chengsong Xie¹, Guoxiang Liu^{1,2}, Lixin Sun¹, Xing-Long Gu¹, Xian Lin¹, Nicole A. Crowley⁴, David Lovinger⁴, and Huaibin Cai^{1,6}

¹Transgenics Section, Laboratory of Neurogenetics, National Institute on Aging, National Institutes of Health, Bethesda, MD 20892

²Feinberg School of Medicine, Northwestern University, Chicago, IL

³Department of Geriatrics, Beijing Geriatric Hospital, Beijing, China 100095

⁴Laboratory of Integrative Neuroscience, National Institute on Alcohol Abuse and Alcoholism, National Institutes of Health, Rockville, MD 20852

Abstract

Leucine-rich repeat kinase 2 (LRRK2) is enriched in the striatal projection neurons (SPNs). Here we show that LRRK2 negatively regulates protein kinase A (PKA) activity in the SPNs during synaptogenesis and in response to dopamine receptor Drd1 activation. LRRK2 interacted with PKA regulatory subunit II β (PKARII β). A lack of LRRK2 promoted the synaptic translocation of PKA and increased PKA-mediated phosphorylation of actin-disassembling enzyme cofilin and glutamate receptor GluR1, resulting in abnormal synaptogenesis and transmission in the developing SPNs. Furthermore, PKA-dependent phosphorylation of GluR1 was also aberrantly enhanced in the striatum of young and aged LRRK2-null mice after treatment with a Drd1 agonist. Notably, a Parkinson's disease-related LRRK2 R1441C missense mutation that impaired the interaction of LRRK2 with PKARII β also induced excessive PKA activity in the SPNs. Our findings reveal a new regulatory role of LRRK2 in PKA signaling, and provide a new pathogenic mechanism of SPN dysfunction in Parkinson's disease.

INTRODUCTION

The impairment of midbrain nigrostriatal dopaminergic innervation at the striatum and the resulting imbalance of striatal output via the direct and indirect pathways underlie the

⁶Correspondence should be addressed either to HC (caih@mail.nih.gov) or LP, (loukia.pariadiou@northwestern.edu).

⁵These authors contributed equally to this work.

AUTHOR CONTRIBUTIONS

L.P and H.C conceived the project, designed the experiments and wrote the manuscript. L.P. and J. Y. generated and analyzed biochemical and cell biology data in Fig. 2–7 and Supplementary Fig. 1–6. J. Y. generated and analyzed data in Fig. 4–7 and Supplementary Fig. S4–6 and performed the Open-field tests in Fig. 7. S.C. and D.L. performed Golgi-COX staining and electrophysiology experiments and data analysis in Fig. 1. G.L and J. Y. performed immunofluorescence experiment of brain section in Supplementary Fig. 2. C.X. conducted primary neuronal cultures, immunofluorescence staining, and transfection experiments. L.S. generated the cofilin constructs shown in Supplemental Fig. 2. X.G. performed the PPF experiment in Fig 1. X.L. was actively involved in the mice generation. N.C. helped with electrophysiology experiments.

neurological basis of Parkinson's disease-related movement disorders¹. Parkinson's disease also causes substantial alterations of the dendritic spine morphology and function of SPNs^{2,3}. The striatum consists of more than 90% of SPNs that are located in two complementary compartments named striosomes and matrix⁴. Notably, LRRK2, one of the most common genetic factors associated with both familial and sporadic Parkinson's disease⁵, is particularly enriched in the striosomal SPNs in contrast to a low expression in the nigrostratal dopaminergic neurons⁶. This distinct expression pattern suggests that LRRK2 may play an important role in the SPNs in response to dopamine stimulation. However, little is known about the pathophysiological functions of LRRK2 in the SPNs under either the normal physiological or disease conditions.

The onset of LRRK2 expression is also coincided with the formation of dendritic spines during neuron development⁷. LRRK2 is involved in actin dynamics that regulates the extension of dendrites and axons in neuron morphogenesis⁸. Dendritic spine formation critical for the connectivity and plasticity in the brain is also determined by the actin cytoskeleton⁹. Spine morphogenesis involves the transition from the initial long, thin, and highly flexible filopodia to the more stable spines that are considered mature when showing characteristic bulbous enlargements (spine head) and a distinct neck¹⁰. Cofilin, a modulator of actin filament turnover, critically regulates the dynamics of spine formation¹¹. Cofilin activity are inhibited by LIM kinase-mediated phosphorylation and stimulated by Slingshot-induced de-phosphorylation on a highly conserved Serine at residue three (S3)¹². However, alternative regulatory mechanisms have been described, including a PKA-dependent pathway¹³.

PKA-mediated signaling pathways are critical for neuron development and function¹⁴. PKA holoenzyme contains two catalytic subunits and two regulatory subunits. Cyclic AMP (cAMP) activates the kinase activity of PKA through disrupting the association between the catalytic and regulatory subunits¹⁵. The mammalian PKA family can be subdivided into types I and II based on their regulatory subunits¹⁶. The PKARII β regulatory subunit is particularly abundant in the SPNs^{17,18}. Dopamine can activate PKA signaling in the SPNs via binding with Drd1-like dopamine receptors¹⁹. The specificity and efficacy of PKA signaling in neurons can also be regulated by A kinase anchoring proteins (AKAPs), which determines the subcellular distribution of PKA holoenzyme by interacting with the regulatory subunits²⁰.

In this study we demonstrate that LRRK2 is a new AKAP-like regulator of the subcellular distribution of PKARII β in neurons, and assign a new physiological role for LRRK2 as a negative modulator of PKA activity in the SPNs during synaptogenesis and in response to dopamine receptor activation. We further investigated the impact of Parkinson's disease-related *LRRK2* missense mutations on the PKA activity and reveal a new pathogenic mechanism of LRRK2 that alters the response of SPNs to dopamine stimulation in the Parkinson's disease-related *LRRK2* R1441C knock-in mice.

RESULTS

LRRK2 regulates the SPN synaptogenesis and transmission

To extend our previous study on the role of LRRK2 in neuron development⁸, we investigated whether LRRK2 affects the dendritic spine formation in the SPNs. Notably, Golgi-COX staining revealed a significant decrease of dendritic spines and increase of dendritic filopodia in the dorsal SPNs of postnatal day 15 (P15) *LRRK2* knockout (*LRRK2*^{-/-}) pups compared to the age-matched wild-type (*LRRK2*^{+/+}) littermate controls (Fig. 1a,b). When the dendritic spines were further categorized as thin, mushroom or stubby based on their maturation stages, a higher proportion of thin and less mushroom spines were found in the *LRRK2*^{-/-} neurons (Fig. 1c). The cumulative frequency distribution analysis showed *LRRK2*^{-/-} SPNs having significantly longer dendritic spines while the spine heads were smaller (Fig. 1d,e). The critical involvement of *LRRK2* in the maturation of dendritic spines is also supported biochemically by the reduction of postsynaptic density (PSD) protein PSD95 expression in striatal extracts of P15 and P21 *LRRK2*^{-/-} mice (Supplementary Fig. 1a,b). We also measured the morphological changes of SPN dendritic spines in 1-month-old *LRRK2*^{-/-} mice. The density and length of the dendritic spines were comparable between *LRRK2*^{+/+} and *LRRK2*^{-/-} neurons, but the diameter of spine heads remains significant smaller in the *LRRK2*^{-/-} neurons (Supplementary Fig. 1c–e). Overall, the loss of *LRRK2* significantly alters the dendritic spine morphology in the SPNs, especially during the developmental stages.

To further examine whether the alteration of spine number and morphology in the *LRRK2*^{-/-} SPNs affects synaptic transmission, we measured glutamatergic miniature excitatory postsynaptic currents (mEPSCs) in striatal slices from P15 *LRRK2*^{-/-} and littermate control *LRRK2*^{+/+} mice by whole-cell voltage clamp recordings (Fig. 1f). While the amplitude of mEPSCs was moderately but significantly increased in *LRRK2*^{-/-} neurons (Fig. 1g), the frequency of mEPSCs was significantly reduced (Fig. 1h). To probe the pre- versus postsynaptic nature of these changes, we recorded the responses of SPNs to paired stimuli, and found that the paired-pulse facilitation (PPF) showed no difference between the genotypes (Fig. 1i). These findings suggest that LRRK2 mainly regulates the postsynaptic response of SPNs.

LRRK2^{-/-} neurons show aberrant phosphorylation of cofilin

We examined the expression level and activity of actin binding proteins in the striatal homogenate of *LRRK2*^{-/-} and age-matched littermate control mice (Supplementary Fig. 2a). We found that while the expression level of total cofilin was comparable, the phosphorylation of cofilin at the conserved residue Serine three (S3) was significantly increased in the P5 to P21 *LRRK2*^{-/-} mouse brains compared to the controls., (Fig. 2a,b; Supplementary Fig. 2a).

Consistently, increased phosphorylation of S3 (pS3) cofilin staining was found in neurons of *LRRK2*^{-/-} hippocampal sections and in the dendritic spine of cultured *LRRK2*^{-/-} hippocampal neurons (Supplementary Fig. 2b, Fig. 2c). Notably, the reduction of pS3 cofilin in the *LRRK2*^{+/+} mice brain was coincided with the increase of LRRK2 expression during

the postnatal development (Fig. 2a), suggesting that LRRK2 may suppress the phosphorylation of cofilin. In agreement with this idea, the levels of pS3 cofilin were reduced in the brain of P2 to P15 *LRRK2* transgenic mice (Supplementary Fig. 2c), which overexpress human wild-type (WT) *LRRK2*²¹. Considering the lack of apparent physical interaction between cofilin and LRRK2 (Supplementary Fig. 2d), LRRK2 may regulate cofilin phosphorylation indirectly through modulating the activity of other protein kinases or phosphatases.

An elevation of pS3 cofilin affects the spine formation

The abnormal increase of pS3 cofilin may impair actin dynamics and spine formation in *LRRK2*^{-/-} neurons. In support of this notion, a significant decrease of filamentous actin (F-actin) content was observed in the dendritic spine of cultured *LRRK2*^{-/-} neurons after 15 days in vitro (DIV) (Fig. 2d,e). The actin cytoskeleton protruding from the dendritic shaft of *LRRK2*^{-/-} neurons appeared thin and elongated (Fig. 2d), which is consistent with a higher incidence of thin filopodia like protrusions found in the P15 *LRRK2*^{-/-} SPNs (Fig. 1a–c).

To establish a direct connection between cofilin phosphorylation and spine morphology, we introduced green fluorescent protein (GFP)-tagged active or inactive forms of cofilin into cultured *LRRK2*^{-/-} or *LRRK2*^{+/+} hippocampal neurons, and examined the alteration of dendritic spine morphology. We found that *LRRK2*^{-/-} neurons transfected with the constitutively active cofilin S3A mutation²² developed more and larger spines and rescued the spine morphology defects in *LRRK2*^{-/-} neurons (Fig. 2f–i). On the contrary, *LRRK2*^{+/+} neurons transfected with the inactive cofilin S3D mutation²² displayed longer and smaller spines with a concomitant increase of filopodia as well as spines with abnormal long protrusions, similar to the alterations observed in *LRRK2*^{-/-} neurons (Fig. 2j–m). These data suggest that the persistent phosphorylation of cofilin in the SPNs of P15 *LRRK2*^{-/-} mice may alter the actin dynamics, resulting in the abnormal dendritic spine morphology.

LRRK2 regulates pS3 cofilin via a PKA-dependent pathway

We next examined the signaling pathways by which LRRK2 regulates cofilin phosphorylation. LIM kinase and Slingshot are typically involved in the phosphorylation and de-phosphorylation of cofilin¹². However, in P15 *LRRK2*^{-/-} pups, no obvious alteration of LIMK1 phosphorylation, an indicator of LIMK1 kinase activity, was found between P15 *LRRK2*^{+/+} and *LRRK2*^{-/-} brain extracts (Supplementary Fig. 3a,b). In addition, the phosphorylated and total levels of Slingshot-1 L (SSH1L), a member of the Slingshot family that dephosphorylates cofilin²³, were also comparable between genotypes (Supplementary Fig. 3a,c). To identify alternative mechanisms of cofilin activity regulated by LRRK2, we compared the levels of pS3 cofilin by Western blot analysis of cultured *LRRK2*^{+/+} and *LRRK2*^{-/-} cortical neurons treated with the activators and inhibitors of various intracellular signaling pathways directly or indirectly related with the regulation of cofilin phosphorylation²⁴. *LRRK2*^{+/+} and *LRRK2*^{-/-} neurons displayed similar changes of cofilin phosphorylation levels in response to modulators of AKT/protein kinase B, phosphoinositide 3-kinase (PI3K), protein kinase C (PKC), mammalian target of rapamycin (mTOR), pyruvate dehydrogenase kinase (PDK1), and MAPK/ERK kinase (MEK) pathways (Supplementary Fig. 3d–g). In contrast, application of forskolin (FSK) that promotes the

production of cAMP and activation of PKA pathway caused a significant increase in cofilin phosphorylation in *LRRK2*^{+/+} neurons, but not in *LRRK2*^{-/-} neurons (Fig. 3a,b). Meanwhile, treatment with a PKA inhibitor PKI resulted in comparable levels of p-cofilin in *LRRK2*^{+/+} and *LRRK2*^{-/-} neurons (Fig. 3c,d). These data suggest an impairment of regulation of PKA signaling in *LRRK2*^{-/-} neurons.

To further confirm these findings, we tested the effect of FSK application on a canonical PKA substrate, cAMP response element-binding protein (CREB) in *LRRK2*^{+/+} and *LRRK2*^{-/-} neurons. FSK treatment induced one-fold increase of phosphorylated CREB (pCREB) in *LRRK2*^{+/+} neurons, but failed to increase the ratio of pCREB in *LRRK2*^{-/-} neurons (Supplementary Fig. 3h-j). In addition, we found a significant increase of pCREB in the nuclear extract of P15 *LRRK2*^{-/-} striatal tissues (Supplementary Fig. 3k,l). All the above suggest an aberrant up-regulation of basal PKA activity in the developing *LRRK2*^{-/-} neurons.

LRRK2 selectively interacts with PKARII β

To determine at which level LRRK2 exerts its effect on PKA activation, we first examined the production of cAMP in cultured *LRRK2*^{+/+} and *LRRK2*^{-/-} neurons treated with vehicle or FSK. In both conditions, no significant difference in cAMP production was observed (Supplementary Fig. 4a,b). We next investigated whether LRRK2 directly interacted with PKA. Co-immunoprecipitation (Co-IP) of LRRK2 with PKA subunits from the striatal extract of human WT *LRRK2* transgenic mice²⁵ revealed a selective interaction between LRRK2 and PKARII β subunit but not with the catalytic subunit (PKAC α) or other regulatory subunits (Fig. 4a). The direct interaction of LRRK2 and PKARII β was further confirmed by an in vitro binding assay using recombinant LRRK2 and PKARII β proteins (Fig. 4b). Although PKA can phosphorylate LRRK2²⁶, no stable direct interaction between LRRK2 and PKAC α recombinant proteins was observed (Fig. 4c). Moreover, endogenous LRRK2 and PKARII β proteins were co-IPed by an LRRK2-specific antibody from the light membrane fraction of *LRRK2*^{+/+} brain homogenates (Fig. 4d), of which both LRRK2 and PKARII β were highly enriched (Supplementary Fig. 4c). Meanwhile, endogenous PKARII β and PKAC α proteins were also co-IPed with LRRK2 by a PKARII β -specific antibody (Fig. 4e), suggesting that LRRK2 co-exists with PKARII β and PKAC α in the same protein complex via direct interaction with PKARII β .

Immunostaining revealed co-localization of endogenous LRRK2 and PKARII β signals in the dendrites of *LRRK2*^{+/+} hippocampal pyramidal neurons (Fig. 4f). While, PKARII β staining was mainly distributed along the dendritic shaft and at the base of dendritic spines in *LRRK2*^{+/+} neurons (Fig. 4g), PKARII β signal was evenly distributed in the dendritic shaft and spines of *LRRK2*^{-/-} neurons (Fig. 4f). Meanwhile, a loss of *LRRK2* did not affect the expression and phosphorylation of PKARII β , the expression of PKAC α , and the association and co-localization of PKARII β with PKAC α in *LRRK2*^{-/-} neurons (Supplementary Fig. 4d-f). Together, these observations suggest that LRRK2 may regulate PKA activity by controlling the subcellular localization of PKARII β along the dendritic shaft.

Further co-IP experiments showed that PKARII β selectively interacted with the Ras of complex proteins (ROC) domain of LRRK2, while, the deletion of the N-terminal two-to-

five residues of PKARII β (PKARII β 2–5) prevented the interaction of PKARII β with LRRK2 (Fig. 4h,4i)..

LRRK2 confines PKARII β to the dendritic shafts

To further investigate the alteration of PKARII β subcellular localization in *LRRK2*^{-/-} neurons (Fig. 4f), we transfected cultured *LRRK2*^{+/+} and *LRRK2*^{-/-} hippocampal neurons with GFP-tagged PKARII β and cell volume marker mCherry. Confocal imaging revealed a predominant presence of PKARII β in the dendritic shafts of *LRRK2*^{+/+} neurons (Fig. 5a). By contrast, a significant increase of dendritic spine PKARII β signal was observed in *LRRK2*^{-/-} neurons (Fig. 5a,b). A similarly increase of GFP-tagged PKAC α in the dendritic spines was also observed in *LRRK2*^{-/-} neurons (Fig. 5c, Supplementary Fig. 5a). Furthermore, subcellular fractionation of P15 mouse forebrain tissues revealed significant increase of PKARII β and PKAC α levels in the postsynaptic density (PSD) fraction of *LRRK2*^{-/-} samples compared to the age-matched *LRRK2*^{+/+} controls (Fig. 5d–f). Therefore, these studies indicate a critical involvement of LRRK2 in controlling the accessibility of PKARII β and PKA holoenzyme into the dendritic spines.

To verify a direct effect of LRRK2 on the subcellular localization of PKARII β , reintroduction of myc-tagged WT *LRRK2* into *LRRK2*^{-/-} neurons prevented the dendritic spine translocation of PKARII β (Supplementary Fig. 5b). Moreover, transfection of PKARII β 2–5 that disrupted the interaction of PKARII β with LRRK2 allowed for the diffusion of PKARII β 2–5 into the dendritic spines of *LRRK2*^{+/+} neurons (Supplementary Fig. 5c). By contrast, linking the MAP2 microtubule-binding domain (MTDB) with PKARII β 2–5, which allows for a direct association of PKARII β 2–5 with the microtubules²⁷, prevented the localization of PKARII β 2–5 into the dendritic spine of *LRRK2*^{+/+} neurons (Supplementary Fig. 5c). Interestingly, PKARII β - 2–5–MTBD was also excluded from the spines of *LRRK2*^{-/-} neurons (Supplementary Fig. 5d), emphasizing the importance of microtubule association in anchoring PKARII β within the dendritic shaft. Considering LRRK2 binds to microtubules and regulates the dynamic assembly of microtubule network^{28,25}, our data further support the importance of the LRRK2 microtubule binding property in providing the structural framework for retaining PKARII β in the dendritic shaft.

Alteration of GluR1 phosphorylation in *LRRK2*^{-/-} neurons

To examine the potential impact of aberrant PKA signaling on the postsynaptic targeting of AMPA-type glutamate receptors, we examined the PKA-dependent phosphorylation of GluR1 at residue Serine 845 (pS845)²⁹. The level of pS845GluR1 was significantly increased in the forebrain homogenate of P5 and P15 *LRRK2*^{-/-} pups compared to the age-matched littermate controls (Fig. 6a,b). The difference in GluR1 phosphorylation disappeared in P30 *LRRK2*^{+/+} and *LRRK2*^{-/-} mice (Fig. 6a,b). FSK treatment did not further increase the level of pS845 GluR1 in cultured *LRRK2*^{-/-} neurons (Supplementary Fig. 6a,b). LRRK2 kinase inhibitor LRRK2-IN-1³⁰ showed no effect on FSK-induced phosphorylation of GluR1 and cofilin in cultured *LRRK2*^{+/+} neurons (Supplementary Fig. 6c–e), suggesting that LRRK2 kinase activity is not involved in regulating PKA activity in neurons.

The phosphorylation of GluR1 by PKA promotes the trafficking of GluR1 to synapses³¹. Although the overall level of GluR1 in the PSD fraction was significantly decreased in the brain homogenate of P15 *LRRK2*^{-/-/-} pups compared to littermate controls (Fig. 6c,d), when normalized against PSD95 protein the level of GluR1 was actually higher in *LRRK2*^{-/-} neurons (Fig. 6e). These observations suggest that *LRRK2*^{-/-} neurons may have less mature dendritic spines, but these mature spines may contain more GluR1 for synaptic transmission.

Dopamine activates the PKA signaling via Drd1 family dopamine receptors¹⁹. Intraperitoneal injection of a selective Drd1 agonist SKF81297³² caused significant increase of pS845 GluR1 in the striatal tissues of P21 *LRRK2*^{+/+} and *LRRK2*^{-/-} mice, whereas significantly more pS845 GluR1 was detected in the *LRRK2*^{-/-} samples (Fig. 6f,g). Furthermore, SKF81297 stimulation also induced more pS845 GluR1 in the striatum of 18-month-old *LRRK2*^{-/-} mice compared to the age-matched controls (Fig. 6h). In contrast, SKF81297 did not affect protein kinase C (PKC)-mediated phosphorylation of GluR1 at S831³³ in the striatum of P21 *LRRK2*^{+/+} and *LRRK2*^{-/-} mice (Supplementary Fig. 6f,g). Taken collectively, these data reveal an aberrant elevation of PKA activity induced by Drd1 activation in both young and aged *LRRK2*^{-/-} mice, suggesting that LRRK2 continues to function as a negative regulator of PKA after the postnatal developmental period.

LRRK2 R1441C mutation impairs its regulatory role on PKA

To examine the impact of Parkinson's disease-related LRRK2 missense mutations on the interaction with PKARII β , we found that the R1441C mutation at the ROC domain of LRRK2 significantly compromised the interaction between LRRK2 and PKARII β (Fig. 7a,b). In vitro recombinant protein binding assays further confirmed the reduced interaction (43.33 7.53%, unpaired t-test, $t_4=7.52$, $p=0.0017$) between R1441C LRRK2 and PKARII β (Fig. 7c). We next examined the effect of R1441C LRRK2 on the subcellular localization of PKARII β in hippocampal neurons cultured from homozygous *LRRK2* R1441C knock-in (*LRRK2*^{R1441C/R1441C}) mice³⁴. A significant increase of PKARII β signals was found in the dendritic spine of *LRRK2*^{KI/KI} neurons compared to the littermate control *LRRK2*^{+/+} neurons (Fig. 7d,e). In addition, *LRRK2*^{R1441C/R1441C} neurons displayed decreased spine area compared to the controls (Fig. 7f). Meanwhile, we also observed a dose-dependent increase of pS3 cofilin and pS845 GluR1 in the brains of P15 *LRRK2*^{+/RC} and *LRRK2*^{R1441C/R1441C} mice (Fig. 7g-j). Together, these data suggest that the R1441C mutation may compromise the regulatory function of LRRK2 on PKA during synaptogenesis.

To test the response of *LRRK2*^{+/R1441C} and *LRRK2*^{R1441C/R1441C} mice to dopamine stimulation, we found that SKF81297 treatment also induced an abnormal increase of pS845 GluR1 in the striatum of P21 and 18-month-old knock-in mice compare to the age-matched control mice (Fig. 7k-m). Notably, both *LRRK2*^{+/RC} and *LRRK2*^{R1441C/R1441C} mice showed similar alterations of GluR1 phosphorylation after treated with SKF81297 (Fig. 7l,m).

To examine the functional consequence of Drd1 activation, we monitored the movement of saline- or SKF81297-treated P21 *LRRK2*^{+/+}, *LRRK2*^{-/-}, and *LRRK2*^{+/R1441C} mice in the Open-field tests. Under the saline treatment, *LRRK2*^{-/-} mice showed significantly increased ambulatory, fine (e.g. grooming), and rearing movements compared to *LRRK2*^{+/+} mice (Fig.

7n–p). Although *LRRK2*^{+/*R1441C*} mice displayed a similar increase of motor activity in the saline-treated condition, the difference is not statistically significant (Fig. 7n–p). The administration of SKF81297 generally promoted the ambulatory and fine movements, but suppressed the rearing of control *LRRK2*^{+/*+*} mice (Fig. 7n–p). Notably, both *LRRK2*^{-/*-*} and *LRRK2*^{+/*R1441C*} mice were significantly less responsive to higher dosage of SKF81297 stimulation compared to the control mice (Fig. 7n–p). These behavioral data suggest that the *LRRK2* R1441C missense mutation may compromise the normal function of *LRRK2* in the SPNs in response to dopamine stimulation.

DISCUSSION

In this study we provide substantial evidence that *LRRK2* regulates synaptogenesis and dopamine receptor activation in the SPNs through modulation of PKA activity. Abnormal dendritic spine morphology and synaptic transmission were observed in the SPNs of P15 *LRRK2*^{-/*-*} pups, which may be attributable to the aberrant increase of PKA-mediated phosphorylation of S3 cofilin, S845 GluR1 and other substrates in the *LRRK2*-deficient neurons. *LRRK2* continues to regulate PKA activity in the SPNs of young and aged mice as evident by the abnormal phosphorylation of S845 GluR1 in response to dopamine receptor *Drd1* activation, which may contribute to the reduced responsiveness of *LRRK2*^{-/*-*} mice to the *Drd1* agonist-induced motor activity. *LRRK2* may regulate the specificity and efficacy of PKA signaling in the SPNs by selectively interacting with PKARII β subunits and controlling the predominantly dendritic shaft localization of PKA holoenzyme. Thereby, a loss of *LRRK2* allowed more translocation of PKA holoenzyme into the dendritic spines where PKA is in closer proximity to the source of cAMP production and the synaptic substrates³⁵, resulting in excessive phosphorylation of key synaptic proteins involving in synaptic formation and transmission. Perhaps more notably, the Parkinson's disease-related *LRRK2* R1441C mutation significantly impaired the interaction between *LRRK2* and PKARII β , and caused similar alterations of PKA signaling as the *LRRK2*-null counterparts. Therefore, our findings provide new molecular insights into the pathophysiological mechanism of *LRRK2* in Parkinson's disease.

In an attempt to identify the molecular players and signaling pathways underlying the dendritic spine morphological changes in *LRRK2*^{-/*-*} neurons, we observed a significant increase of cofilin phosphorylation in these neurons. The phosphorylation of cofilin is generally accepted to decrease its binding with F-actin and prevent its disassembly of F-actin³⁶. Consistent with an earlier study³⁷, the decrease of cofilin activity in *LRRK2*^{-/*-*} neurons impaired the dynamic assembly of F-actin as evident by the accumulation of F-actin aggregates in the soma and the decrease of F-actin content in the dendritic spines. Accordingly, the introduction of constitutively active S3A-cofilin in *LRRK2*^{-/*-*} neurons prevented F-actin aggregation. The inhibition of cofilin activity by siRNA knockdown has also been shown to cause longer, thinner, and more complex dendritic protrusions in cultured neurons³⁸, as we have observed in the *LRRK2*^{-/*-*} neurons. Collaboratively, the introduction of S3A-cofilin enabled to rescue the dendritic spine abnormalities in the *LRRK2*^{-/*-*} neurons. It is worth to point out that cofilin not only depolymerizes or severs F-actin according to the classical model, it also promotes the net assembly and polymerization of the newly generated barbed ends under specific conditions³⁹, which may explain how the

inactivation of cofilin led to aggregation of F-actin at the soma and reduced the F-actin content in the dendritic spine of *LRRK2*^{-/-} neurons. Together, our observations reveal an active involvement of LRRK2 in the formation of dendritic spines through modulating cofilin-mediated actin dynamics.

LRRK2 modulates the activity of PKA α by anchoring both PKA α and PKARII β along the dendritic shaft. The spatial restriction of PKARII β in the dendritic shaft plays an important role in regulating PKA α activity during the excitatory synaptic transmission²⁷. For instance, dendritic MAP2 is considered as a neuronal AKAP that anchors PKARII β along with PKA α in the dendritic shaft⁴⁰. After cAMP binds to PKARII β , the catalytic subunits begin to dissociate from the complex and enter the dendritic spine²⁷. Neurons derived from *MAP2 1-158* mutant mice that also display increased translocation of PKARII β into dendritic spines show increase of PKA-dependent phosphorylation of GluR1²⁷. Based on these previous observations^{27,40} we propose LRRK2 as an additional dendritic AKAP that interacts with PKARII β , acting synergistically with, or independently of MAP2, particularly at the time of active dendritic spine morphogenesis. Similarly to what happened in the *MAP2 1-158* mutant mice⁴⁰, the absence of LRRK2 allowed significantly more PKA α and PKARII β subunits in the dendritic spines of *LRRK2*^{-/-} neurons, which is likely to bring PKA holoenzyme closer to the upstream components of cAMP-mediated signaling transduction pathways, such as the dopamine receptors and adenylylase, as well as the downstream substrates, such as the synaptic protein GluR1, resulting in the abnormally increased PKA activity. Therefore, there may exist competition between dendritic shaft AKAPs, such as MAP2 and LRRK2, and synaptic AKAPs such as AKAP79/150⁴¹, in anchoring the PKA holoenzyme in the dendritic shaft and spines. The loss of LRRK2 may shift the balance to more PKA binding with the synaptic AKAPs, leading to more PKA activity. This hypothesis is further supported by a recent computational analysis of the importance of subcellular location of PKA holoenzyme in dopamine receptor *Drd1*-induced activation of PKA³⁵. The key revelation of this study is that cAMP exhibits a strong spatial gradient within the dendritic spines and shaft upon dopamine activation, of which the distance between PKA and the source of cAMP is more important in controlling the PKA activity. Given the presence of *Drd1* receptor, G protein (G_{off}), and adenylylase 5 (*AC5*) mainly in the dendritic spines of SPNs³⁵, the increase translocation of PKA holoenzyme in the spines of *LRRK2*^{-/-} SPNs thereby renders these neurons more sensitive to PKA activation in response to dopamine stimulation.

Considering the predominant effects of LRRK2 occurs between P5 and P15, LRRK2 may be a key negative regulator of PKA signaling at this critical time period for synaptogenesis. In line with this notion, PKARII β is important for the induction of LTP in young mice (P10–P14) but not in older ones (P21–P28), of which another protein kinase CaMKII becomes predominant⁴². Having shown morphological changes in dendritic spines as a result of *LRRK2*'s absence, we examined excitatory synaptic transmission in *LRRK2*^{-/-} neurons. We demonstrate a decrease in the frequency of mEPSCs in the SPNs of P15 pups that may reflect the improper maturation of dendritic spines and synapses in these neurons. This observation is further supported by the decrease in the expression of synaptic markers such as the postsynaptic adaptor proteins PSD95 in the PSD fraction of P15 *LRRK2*^{-/-} brains. On

the other hand, the amplitude of the mEPSCs was slightly but significantly increased in P15 *LRRK2*^{-/-} neurons, despite the overall decrease in GluR1 level in the PSD fraction. However, provided that *LRRK2*^{-/-} neurons had less PSD proteins, further normalization of GluR1 against PSD95 protein showed an actual increase of GluR1 in the PSD fraction of *LRRK2*^{-/-} mice. Therefore, *LRRK2*^{-/-} neurons had overall less mature dendritic spines and synapses, but their mature spines contained more GluR1, resulting in reduced mEPSC frequency but increased mEPSC amplitude. These data are also of interest considering that increased GluR1 phosphorylation is observed in the P5 and P15 *LRRK2*^{-/-} pups. Enhanced GluR1 phosphorylation may facilitate its trafficking to the perisynaptic sites followed by lateral diffusion into the dendritic spines⁴³, which may lead to more GluR1 targeted to the postsynaptic site of mature dendritic spines in *LRRK2*^{-/-} neurons. The increased synaptic targeting of GluR1 as well as the related increase of mEPSC amplitude may serve as a compensatory mechanism to salvage the overall impaired synaptic transmission due to the delay of spine maturation in *LRRK2*^{-/-} neurons.

The impairment of synaptic transmission underlies the key pathophysiological phenotypes prior to neurodegeneration in Alzheimer's disease, Parkinson's disease, and other degenerative neurological disorders⁴⁴. Parkinson's disease-related dopamine deficiency has been shown to cause substantial changes of the spine morphology and function of SPNs³. Golgi staining of postmortem Parkinson's disease brains has revealed 20–30% reduction in striatal spine density and a reduction of the size of the dendritic trees of SPNs^{45,46}. Together, these early studies demonstrate a critical involvement of SPNs in the pathogenic processes of Parkinson's disease. In light of the function of LRRK2 in regulating PKA activity, Drd1 in the SPNs also utilizes the PKA pathway as a means to relay extracellular dopamine stimulation to intracellular signaling transduction¹. It also should be noted that phenotypes of PKARII β knockout mice are mainly related to the striatal functions, emphasizing the requirement of PKARII β in motor learning and related dopaminergic signaling¹⁸. Therefore, we suspect that *LRRK2*-deficiency may interfere with the PKA signaling in the striatal SPNs and compromise their responses to dopaminergic transmission. Indeed, Drd1 agonist caused aberrant increase of PKA-mediated phosphorylation of GluR1 in the striatum of *LRRK2*^{-/-} mice, which may be attributable to the less responsiveness of *LRRK2*^{-/-} mice to Drd1 agonist-induced motor activity. Interestingly, Parkinson's disease-related *LRRK2* R1441C knock-in mice showed similar abnormal GluR1 phosphorylation and motor behavioral phenotypes as the *LRRK2*^{-/-} mice in responding to Drd1 stimulation. These observations are also consistent with an early report that *LRRK2* R1441C knock-in mice are less responsive to amphetamine-induced locomotor activity³⁴, as the main effect of amphetamine in the striatum is to causes an increase of dopamine release⁴⁷. Considering LRRK2 functions as a dimer⁴⁸, our data suggest the R1441C missense mutation may exert a dominant-negative effect on the regulatory function of LRRK2 in modulating PKA activity by dimerization with the wild-type proteins.

The activation of Drd1 appears to exert different effects on different types of motor activities, which increased the ambulatory and fine movements, but suppressed the rearing, suggesting the existence of different Drd1-involved neural circuits in regulating specific motor outputs. The loss of LRRK2 mainly compromised the ambulatory and fine motor

responses to *Drd1* activation. Given *LRRK2* is more abundant in a subset of SPNs at the striosomes⁶, it is of interest to determine the exact neural circuits in the striatum and basal ganglion affected by *LRRK2*. Notably, a recent neural tracing study reveals that SPNs in the striosomes can directly project to the nigrostriatal dopaminergic neurons⁴⁹. Although the functionality of this newly defined circuit remains to establish, SPNs in the striosomes may directly modulate the excitability and dopamine release of nigrostriatal dopaminergic neurons. Considering the increase of pS845 GluR1 in the *LRRK2*^{-/-} and *LRRK2*^{+R1441C} SPNs may enhance the postsynaptic transmission and activation of these inhibitory GABAergic neurons, we suspect that *LRRK2*^{-/-} and *LRRK2*^{+R1441C} SPNs may further inhibit the activity of nigrostriatal dopaminergic neurons, resulting in suppression of dopamine release. Certainly, more physiological and behavioral studies will need to fully understand the function of this circuit in both normal and Parkinson's disease conditions.

ONLINE METHODS

Animals

LRRK2^{-/-} mice, *CaMKII-tTA/tetO-WT-LRRK2* transgenic mice, *LRRK2* wild-type BAC transgenic mice and *LRRK2* R1441C knock-in mice were created as described previously^{8,21,25,34}, and maintained in C57BL6 strain background. Two to four mice were housed in each cages and in a 12h light/dark cycle and fed regular diet *ad libitum*. All mouse work follows the guidelines approved by the Institutional Animal Care and Use Committees of the National Institute of Child Health and Human Development, NIH.

Golgi–Cox impregnation of brain tissue and spine measurements

Mice were perfused intracardially with 0.9% saline. The brains were dissected, and impregnated using a standard Golgi–Cox solution (1% potassium dichromate, 1% mercuric chloride, and 0.8% potassium chromate), according to a previously described method⁵⁰. The brains immersed in the Golgi–Cox solution were stored at room temperature for 6d, immersed in a sucrose solution (30%) for 2d, and sectioned coronally (150 μ m) using a vibratome. Sections were mounted on gelatinized slides and stained according to a previously described method⁵¹. Dorsolateral striatal Golgi-stained sections were imaged under brightfield illumination on a Zeiss microscope system and a 100 \times oil immersion lens. Healthy SPNs were chosen randomly for quantification from three mice per group, and spines on tertiary dendrites were considered from an individual blind to the genotype of neurons. The density of spines and filopodia was analyzed by NeuroLucida 10 software (MBF Inc., Williston, VT, USA). For spine size, images were acquired and the full length and head diameter were measured manually with ImageViewer⁵², a custom-made software for spine analysis written in Matlab (The MathWorks). For frequency distributions, spines were separated into thin mushroom and stubby spines based on length to head width ratio. Each spine was categorized as stubby if without a neck, and with a total length to head width ratio less than 0.3. Spines with total length to head width ratio more than 1 were categorized as thin, and those between 0.31 and 0.99 were categorized as mushroom. Filopodia were protrusions greater than 2.5 μ m in length without a neck. The comparison of cumulative frequency distributions was evaluated by the Kolmogorov-Smirnov test (KS-test), and average comparison of length, width and densities were performed with Student's t test or U

of Mann-Whitney test. Distributions in frequencies of different category of spine were compared with Chi-Squared test.

Electrophysiology

Brain slices containing striatum were prepared from P14–15 or P21–28 *LRRK2*^{-/-} and *LRRK2*^{+/+} littermates. The animals were anesthetized deeply with isoflurane and decapitated. The brains were placed in ice-cold modified artificial CSF (aCSF) containing the following: 194mM sucrose, 30mM NaCl, 4.5mM KCl, 1mM MgCl₂, 26mM NaHCO₃, 1.2mM NaH₂PO₄, and 10mM dextrose, saturated with 95% O₂/5% CO₂. Coronal sections (280µm) through striatum were prepared using a vibratome (Leica Microsystems). Sections were equilibrated for at least 1h at 33°C in 95% O₂/5% CO₂ continuously bubbled aCSF containing the following: 124mM NaCl, 4.5mM KCl, 2mM CaCl₂, 1mM MgCl₂, 26mM NaHCO₃, 1.2mM NaH₂PO₄, and 10mM D-glucose. Sections were subsequently incubated in the same solution at room temperature. Electrodes (2–5MΩ resistance) were pulled from borosilicate glass on a Flaming/Brown micropipette puller (Sutter Instruments). Pipettes were filled with solution (290–300mOsm) containing the following: 120mM CsMeSO₃, 5mM NaCl, 10mM tetraethylammonium-Cl, 10mM HEPES, 5mM QX-314, 1.1mM EGTA, 0.3mM Na-GTP, and 4mM Mg-ATP, with pH set at 7.2 with CsOH⁵³. Miniature EPSCs (mEPSCs) were performed between 29°C and 31°C and in the presence of picrotoxin (50µM) and TTX (1µM). Currents were measured in conventional ruptured-patch whole-cell mode in striatal medium spiny neurons (SPNs) voltage-clamped at –60mV using a Multiclamp 700A amplifier (Molecular Devices). mEPSCs were recorded in gap-free mode for 5–10min and analyzed by using the Mini Analysis Program (Synaptosoft Inc)⁵⁴ [Amplitude threshold (15), Area threshold (20), Period to search local maximum (15000µs), Time before peak for baseline (10000µs), Period to average baseline (10000µs), Period to search decay time (5000µs), Fraction to find decay (0.001)]. To measure paired pulse facilitation (PPF), recordings were performed in the presence of picrotoxin (100µM). Paired stimuli at an interpulse interval of 50ms were delivered and the ratio of peak amplitudes of the EPSCs was calculated.

Western blot and co-IP

Tissue or neurons were lysed in 50mM Tris-HCl pH7.6, 150mM NaCl, 2mM EDTA, 2% SDS or RIPA buffer (Sigma Aldrich) supplemented with complete protease inhibitor mixture (Roche Applied Biosciences) and phosphatase inhibitor mixture (Pierce Biotechnology). Proteins were separated by 4–12% NuPage Bis-Tris PAGE (Invitrogen) and transferred to nitrocellulose membranes. Antibodies specific for LRRK2 [Epitomics 3514-1, IP 1:1000; UC Davis/NIH NeuroMab Facility 73–188, Western blot (WB) 1:1000, immunocytochemistry (ICC) 1:200; and Abcam ab133475, WB 1:1000, ICC 1:200], pLRRK2 (S935, Abcam ab133450, WB 1:1000), PKACα (BD Bioscience 610981, WB 1:1000 and Cell Signaling 47825, IP 1:1000, WB 1:1000, ICC 1:1000), PKARIα (BD Biosciences 51-9002044, WB 1:1000), PKARIIα (BD Biosciences 51-9002051, WB 1:1000), PKARIIβ (BD Biosciences 610625, WB 1:10000, ICC 1:1000, IP: 1:1000), pPKARIIβ (S114, BD Biosciences 612550, WB 1:1000), pCofilin [S3, Cell Signaling 3313S, WB 1:1000, ICC 1:200, immunohistochemistry (IHC), 1:200], Cofilin (cell Signaling 3318, WB 1:1000), pLIMK1 (T508, Cell Signaling 3841, WB 1:1000), LIMK1

(Cell Signaling 3842, WB 1:1000), Hsp90 (BD Biosciences 610418, WB 1:1000), pCREB (S133, Cell Signaling 9198, WB 1:1000), CREB (Cell Signaling 9104, WB 1:1000), pGluR1 (S845, Sigma A4477, WB 1:1000; S831, Sigma A4352, WB 1:1000), GluR1 (Abcam ab31232, WB 1:1000), β -actin (Sigma A2228, WB 1:1000), PSD95 (Sigma P246, WB 1:1000; Millipore MAB1598, ICC 1:200), PP1 (Sigma P7607, WB 1:1000), 14-3-3 ζ (Cell Signaling 7413, WB 1:1000), HA (Roche Applied Science 11867423001, WB 1:1000), myc (Sigma M4439, WB 1:1000, IP 1:1000), pSSH1L (S978, ECM Biosciences SP3901, WB 1:1000), SSH1L (ECM Biosciences SP1711, WB 1:1000), β -tubulin III (Millipore AB9345, WB 1:1000), Diap1 (Cell Signaling 5486P, WB 1:1000), Diap2 (Cell Signaling 5474P, WB 1:1000), Arp2 (Cell Signaling 3128P, WB 1:1000), Arp3 (Cell Signaling 4738P, WB 1:1000), CAP1 (Sigma, SAB1406999, WB 1:1000), and cdc42/Rac (Cell Signaling 2416, WB 1:1000) were used. Protein bands were detected using the enhanced chemiluminescence (ECL) system (Pierce Biotechnology) and quantified using the Scion Image System. For the co-immunoprecipitation experiments, brain extracts or cellular extracts of transfected cells (500–1500 μ g of total protein) were lysed with IP buffer (20mM Hepes, 300mM NaCl, 5% (v/v) glycerol, 0.2mM EDTA and 1% NP40). The lysates were incubated with appropriate dilutions of the various antibodies overnight at 4°C. Antibody-bound protein complexes were collected with either protein G or protein A (Pierce Rockford, IL, USA) for 1h at 4 °C, and then the pellets were washed five times with IP buffer at 4°C. The beads were resuspended in SDS sample buffer (Invitrogen) and the recovered proteins were separated by SDS-PAGE gel electrophoresis, and detected by immunoblot analysis.

Primary neuronal cell cultures

Primary neuronal cultures from cortex, striatum and hippocampus from pups at P0 were prepared as described previously⁵⁵. In brief, neurons were dissociated by papain buffer (Sigma Aldrich), and were then placed in poly-D-lysine slides (BD) or plates in Basal Eagle Medium (Sigma-Aldrich). Arabinosylcytosine (Sigma-Aldrich) was used to inhibit glial cell growth. Forskolin (FSK), PKI (PKA inhibitor) and LRRK2 kinase inhibitor LRRK2-IN-1 (Tocris Bioscience, Bristol, UK) as well as all the other compounds were added directly to the medium of cortical neurons from stock solution and unless otherwise stated these compounds were from Calbiochem.

Transfection of primary neurons

Primary hippocampal or striatal neurons were transfected between P15-P21 DIV using the calcium phosphate method as described previously⁵⁶. Neuronal cultures were incubated with the DNA-calcium phosphate precipitate for approximately 1.5hr. The precipitate was then dissolved by the incubation of the cells in a medium that had been pre-equilibrated in a 10% CO₂ incubator. The cells were in turn transferred to their original conditioned medium and fixed at about 24–48hr after transfection. GFP-tagged PKARII β , PKAC α , PKARII β 2–5, and PKARII β 2–5 expression vector and mCherry expression construct were obtained from Dr. Haining Zhong. Myc-tagged human wild-type *LRRK2* and *LRRK2* ROC domain expression constructs were obtained from Dr. Mark Cookson (NIA, NIH). GFP-tagged cofilin expression vector was purchased from Origene Technologies (Rockville, MD). GFP-S3A and GFP-S3D cofilin mutant constructs were generated using QuikChange II Site-Directed Mutagenesis Kit (Agilent Technologies, Santa Clara, CA).

Immunofluorescence staining and image acquisition

Neurons were fixed in 4% paraformaldehyde (PFA) as described previously⁸. Briefly, they were permeabilized with Triton-X-100 and incubated with 10% goat serum (Sigma-Aldrich) for 1hr to block unspecific binding and incubated overnight with the primary antibody. Fluorescent images were captured using a Zeiss confocal microscope (LSM510META). Spinal intensities and areas quantification was performed using the Image J Software. Regions of interest (ROIs) were set up automatically and the green (PKARII β) and red (mCherry) signals within the ROIs were divided to adjacent dendritic green and red intensities. The ratio of the normalized green to red signals in each genotype represents the relative intensity of the PKARII β inside the spines. The data presented involve about 80–150 spines sampled from three randomly selected microscopic fields of at least three independent experiments from a person blind to the genotype of neurons.

cAMP ELISA determination

cAMP levels of cortical neurons of each genotype (*LRRK2*^{+/+}, *LRRK2*^{-/-}) treated or untreated with FSK were quantified by using a cAMP Elisa kit (R&D Systems) according to the manufacturer's protocol. Briefly, three independent experiments with each sample assaying in duplicates were used for the analysis. The goat anti-mouse antibody that is coated on the microplate binds to a monoclonal antibody specific for cAMP. The cAMP present in the samples compete with an amount of HRP-labeled cAMP for binding on the monoclonal antibody. A substrate solution is incubated in the microplate to determine the bound enzyme activity. The intensity of the color is proportional to the cAMP inverse concentration to the concentration of cAMP in the sample.

Subcellular fractionation of brains

PSD fractions were prepared from mouse brains as previously described⁵⁷. All procedures performed at 4°C. Mouse brains were rapidly decapitated and homogenized in four volumes of ice-cold Buffer A (0.32M sucrose, 5mM HEPES, pH7.4, 1mM MgCl₂, 0.5mM CaCl₂, protease and phosphatase inhibitor mixture) with Teflon homogenizer (12 strokes). Homogenized brain extract was spun at 1400 × *g* for 10min. Supernatant (S1) was saved and pellet (P1) was homogenized again with Teflon homogenizer with buffer A (5 strokes). After centrifugation at 700 × *g*, the supernatant (S1') was saved and pooled with S1. Pooled S1 and S1' were centrifuged at 13,800 × *g* for 10min to collect the crude synaptosomal pellet (P2) and the supernatant (S2), which contains the cytosol and light membranes. S2 was centrifuged at 100,000 × *g* for 15min to produce the cytosolic fraction (S2') and the light membrane (LM) fraction. P2 was resuspended in Buffer B (0.32M sucrose, 6mM Tris, pH 8.0 supplemented with protease and phosphatase inhibitors cocktail) with Teflon homogenizer (five strokes). The P2 suspension was loaded onto a discontinuous sucrose gradient (0.85M/1M/1.15M sucrose solution in 6mM Tris, pH8.0), followed by centrifugation for 2h at 82,500 × *g*. The synaptosome fraction between 1M and 1.15M sucrose was collected and resuspended with 6mM Tris with 0.5% Triton. The PSD fraction was purified by centrifugation at 18,900 rpm with a Ti70.1 rotor.

Intraperitoneal injection of Drd1 agonist SKF-81297, Open-field test, and Western blot analysis of striatal proteins

Healthy mice removed from the light cycle were placed in the dark room for 30min before behavioral test. 5min after the intraperitoneal injection of 0.9% (w/v) saline, 2mg/kg or 10mg/kg Drd1 agonist, R(+)-SKF-81297 hydrobromide (Sigma), mice were placed in the chamber for Open-field test using Flex-Field activity system (San Diego Instruments, CA) as described previously^{32,58}. Immediately after the behavioral test, mice were decapitated and the striatal tissues were dissected out. Striatal tissues were homogenized and sonicated in 1% SDS lysis buffer and denatured at 70°C for 10min, as described previously⁵⁹. 20ug protein was resolved in 4–12% Tris-Bis NuPage gel and transferred to PVDF membrane. Blots were incubated with antibodies against total GluR1 and pS845 GluR1. Expression level and the ratios between phosphorylated and total proteins were determined using a LI-COR system and Odyssey software and expressed relative to saline vehicle controls.

Statistics

Graph Pad Prism 5 was used for the Statistical Analysis. Statistical significances were determined by comparing means of different groups using *t* test or two-way ANOVA followed by post-tests. Distributions of mEPSC amplitudes and frequencies as well as morphological analysis distributions were compared using Chi-Squared test or Kolmogorov-Smirnov (K-S) tests. Band intensities of Western blots were compared with unpaired Student *t*-tests (two-sided). Summary data is presented as mean SEM. **P*<0.05; ***p*<0.01; ****p*<0.001, *****p*<0.0001.

Supplementary Material

Refer to Web version on PubMed Central for supplementary material.

Acknowledgments

This work was supported by the intramural research programs of National Institute on Aging (AG000944, AG000928, HC) and National Institute of Alcohol Abuse and Alcoholism (DL). We thank Dr. Haining Zhong of Vollum Institute for providing *PKA* expression vectors, Dr. Mark Cookson of NIA for providing human *LRRK2* expression vector, Drs. Jie Shen and Youren Tong of Harvard University for providing *LRRK2* R1441C knock-in mice, Dr. Patrick Lewis of University College London for providing *LRRK2* wild-type and R1441C recombinant proteins, Dr. Veronica Alvarez from NIAAA, Dr. Bo Ma from NIA and Drs. Zheng Li, Jie-Min Jia, and Song Jiao of National Institute of Mental Health for their advice and technical support. We also thank Ms. Laura Donahue and Ms. Namratha Sastry for their assistance in editing the manuscript.

References

1. Gerfen CR, Surmeier DJ. Modulation of striatal projection systems by dopamine. *Annu Rev Neurosci.* 2011; 34:441–466.10.1146/annurev-neuro-061010-113641 [PubMed: 21469956]
2. Smith Y, Villalba RM, Raju DV. Striatal spine plasticity in Parkinson's disease: pathological or not? *Parkinsonism Relat Disord.* 2009; 15(Suppl 3):S156–161.10.1016/S1353-8020(09)70805-3 [PubMed: 20082980]
3. Calabresi P, Picconi B, Tozzi A, Di Filippo M. Dopamine-mediated regulation of corticostriatal synaptic plasticity. *Trends Neurosci.* 2007; 30:211–219.10.1016/j.tins.2007.03.001 [PubMed: 17367873]
4. Graybiel AM, Ragsdale CW Jr, Moon Edley S. Compartments in the striatum of the cat observed by retrograde cell labeling. *Exp Brain Res.* 1979; 34:189–195. [PubMed: 759226]

5. Singleton AB, Farrer MJ, Bonifati V. The genetics of Parkinson's disease: progress and therapeutic implications. *Movement disorders : official journal of the Movement Disorder Society*. 2013; 28:14–23.10.1002/mds.25249 [PubMed: 23389780]
6. Mandemakers W, Snellinx A, O'Neill MJ, de Strooper B. LRRK2 expression is enriched in the striosomal compartment of mouse striatum. *Neurobiol Dis*. 2012; 48:582–593.10.1016/j.nbd.2012.07.017 [PubMed: 22850484]
7. Westerlund M, et al. Developmental regulation of leucine-rich repeat kinase 1 and 2 expression in the brain and other rodent and human organs: Implications for Parkinson's disease. *Neuroscience*. 2008; 152:429–436.10.1016/j.neuroscience.2007.10.062 [PubMed: 18272292]
8. Parisiadou L, et al. Phosphorylation of ezrin/radixin/moesin proteins by LRRK2 promotes the rearrangement of actin cytoskeleton in neuronal morphogenesis. *J Neurosci*. 2009; 29:13971–13980.10.1523/JNEUROSCI.3799-09.2009 [PubMed: 19890007]
9. Tada T, Sheng M. Molecular mechanisms of dendritic spine morphogenesis. *Curr Opin Neurobiol*. 2006; 16:95–101.10.1016/j.conb.2005.12.001 [PubMed: 16361095]
10. Yoshihara Y, De Roo M, Muller D. Dendritic spine formation and stabilization. *Curr Opin Neurobiol*. 2009; 19:146–153.10.1016/j.conb.2009.05.013 [PubMed: 19523814]
11. Meng Y, et al. Abnormal spine morphology and enhanced LTP in LIMK-1 knockout mice. *Neuron*. 2002; 35:121–133. [PubMed: 12123613]
12. Bernstein BW, Bamburg JR. ADF/cofilin: a functional node in cell biology. *Trends Cell Biol*. 2010; 20:187–195.10.1016/j.tcb.2010.01.001 [PubMed: 20133134]
13. Nadella KS, et al. Regulation of actin function by protein kinase A-mediated phosphorylation of Limk1. *EMBO Rep*. 2009; 10:599–605.10.1038/embor.2009.58 [PubMed: 19424295]
14. Frey U, Huang YY, Kandel ER. Effects of cAMP simulate a late stage of LTP in hippocampal CA1 neurons. *Science*. 1993; 260:1661–1664. [PubMed: 8389057]
15. Francis SH, Corbin JD. Structure and function of cyclic nucleotide-dependent protein kinases. *Annu Rev Physiol*. 1994; 56:237–272.10.1146/annurev.ph.56.030194.001321 [PubMed: 8010741]
16. Brandon EP, Idzerda RL, McKnight GS. PKA isoforms, neural pathways, and behaviour: making the connection. *Curr Opin Neurobiol*. 1997; 7:397–403. [PubMed: 9232801]
17. Ventra C, et al. The differential response of protein kinase A to cyclic AMP in discrete brain areas correlates with the abundance of regulatory subunit II. *J Neurochem*. 1996; 66:1752–1761. [PubMed: 8627334]
18. Brandon EP, et al. Defective motor behavior and neural gene expression in RIIbeta-protein kinase A mutant mice. *J Neurosci*. 1998; 18:3639–3649. [PubMed: 9570795]
19. Snyder GL, Fienberg AA, Haganir RL, Greengard P. A dopamine/D1 receptor/protein kinase A/dopamine- and cAMP-regulated phosphoprotein (Mr 32 kDa)/protein phosphatase-1 pathway regulates dephosphorylation of the NMDA receptor. *J Neurosci*. 1998; 18:10297–10303. [PubMed: 9852567]
20. Wong W, Scott JD. AKAP signalling complexes: focal points in space and time. *Nat Rev Mol Cell Biol*. 2004; 5:959–970.10.1038/nrm1527 [PubMed: 15573134]
21. Li Y, et al. Mutant LRRK2(R1441G) BAC transgenic mice recapitulate cardinal features of Parkinson's disease. *Nat Neurosci*. 2009; 12:826–828.10.1038/nn.2349 [PubMed: 19503083]
22. Nagaoka R, Abe H, Obinata T. Site-directed mutagenesis of the phosphorylation site of cofilin: its role in cofilin-actin interaction and cytoplasmic localization. *Cell Motil Cytoskeleton*. 1996; 35:200–209.10.1002/(SICI)1097-0169(1996)35:3<200::AID-CM3>3.0.CO;2-C [PubMed: 8913641]
23. Niwa R, Nagata-Ohashi K, Takeichi M, Mizuno K, Uemura T. Control of actin reorganization by Slingshot, a family of phosphatases that dephosphorylate ADF/cofilin. *Cell*. 2002; 108:233–246. [PubMed: 11832213]
24. Gungabissoon RA, Bamburg JR. Regulation of growth cone actin dynamics by ADF/cofilin. *J Histochem Cytochem*. 2003; 51:411–420. [PubMed: 12642619]
25. Lin X, et al. Leucine-rich repeat kinase 2 regulates the progression of neuropathology induced by Parkinson's-disease-related mutant alpha-synuclein. *Neuron*. 2009; 64:807–827.10.1016/j.neuron.2009.11.006 [PubMed: 20064389]

26. Li X, et al. Phosphorylation-dependent 14-3-3 binding to LRRK2 is impaired by common mutations of familial Parkinson's disease. *PLoS One*. 2011; 6:e17153.10.1371/journal.pone.0017153 [PubMed: 21390248]
27. Zhong H, et al. Subcellular dynamics of type II PKA in neurons. *Neuron*. 2009; 62:363–374.10.1016/j.neuron.2009.03.013 [PubMed: 19447092]
28. Gandhi PN, Wang X, Zhu X, Chen SG, Wilson-Delfosse AL. The Roc domain of leucine-rich repeat kinase 2 is sufficient for interaction with microtubules. *J Neurosci Res*. 2008; 86:1711–1720.10.1002/jnr.21622 [PubMed: 18214993]
29. Blackstone C, Murphy TH, Moss SJ, Baraban JM, Haganir RL. Cyclic AMP and synaptic activity-dependent phosphorylation of AMPA-preferring glutamate receptors. *J Neurosci*. 1994; 14:7585–7593. [PubMed: 7527845]
30. Deng X, et al. Characterization of a selective inhibitor of the Parkinson's disease kinase LRRK2. *Nat Chem Biol*. 2011; 7:203–205.10.1038/nchembio.538 [PubMed: 21378983]
31. Esteban JA, et al. PKA phosphorylation of AMPA receptor subunits controls synaptic trafficking underlying plasticity. *Nat Neurosci*. 2003; 6:136–143.10.1038/nn997 [PubMed: 12536214]
32. Kim DS, Szczypka MS, Palmiter RD. Dopamine-deficient mice are hypersensitive to dopamine receptor agonists. *J Neurosci*. 2000; 20:4405–4413. [PubMed: 10844009]
33. Roche KW, O'Brien RJ, Mammen AL, Bernhardt J, Haganir RL. Characterization of multiple phosphorylation sites on the AMPA receptor GluR1 subunit. *Neuron*. 1996; 16:1179–1188. [PubMed: 8663994]
34. Tong Y, et al. R1441C mutation in LRRK2 impairs dopaminergic neurotransmission in mice. *Proceedings of the National Academy of Sciences of the United States of America*. 2009; 106:14622–14627.10.1073/pnas.0906334106 [PubMed: 19667187]
35. Oliveira RF, Kim M, Blackwell KT. Subcellular location of PKA controls striatal plasticity: stochastic simulations in spiny dendrites. *PLoS Comput Biol*. 2012; 8:e1002383.10.1371/journal.pcbi.1002383 [PubMed: 22346744]
36. Bamburg JR, Bernstein BW. ADF/cofilin. *Curr Biol*. 2008; 18:R273–275.10.1016/j.cub.2008.02.002 [PubMed: 18397729]
37. Bellenchi GC, et al. N-cofilin is associated with neuronal migration disorders and cell cycle control in the cerebral cortex. *Genes Dev*. 2007; 21:2347–2357.10.1101/gad.434307 [PubMed: 17875668]
38. Hotulainen P, et al. Defining mechanisms of actin polymerization and depolymerization during dendritic spine morphogenesis. *J Cell Biol*. 2009; 185:323–339.10.1083/jcb.200809046 [PubMed: 19380880]
39. Andrianantoandro E, Pollard TD. Mechanism of actin filament turnover by severing and nucleation at different concentrations of ADF/cofilin. *Mol Cell*. 2006; 24:13–23.10.1016/j.molcel.2006.08.006 [PubMed: 17018289]
40. Harada A, Teng J, Takei Y, Oguchi K, Hirokawa N. MAP2 is required for dendrite elongation, PKA anchoring in dendrites, and proper PKA signal transduction. *J Cell Biol*. 2002; 158:541–549.10.1083/jcb.200110134 [PubMed: 12163474]
41. Bauman AL, Goehring AS, Scott JD. Orchestration of synaptic plasticity through AKAP signaling complexes. *Neuropharmacology*. 2004; 46:299–310.10.1016/j.neuropharm.2003.09.016 [PubMed: 14975685]
42. Yasuda H, Barth AL, Stellwagen D, Malenka RC. A developmental switch in the signaling cascades for LTP induction. *Nat Neurosci*. 2003; 6:15–16.10.1038/nn985 [PubMed: 12469130]
43. He K, et al. Stabilization of Ca²⁺-permeable AMPA receptors at perisynaptic sites by GluR1-S845 phosphorylation. *Proceedings of the National Academy of Sciences of the United States of America*. 2009; 106:20033–20038.10.1073/pnas.0910338106 [PubMed: 19892736]
44. Shen J. Impaired neurotransmitter release in Alzheimer's and Parkinson's diseases. *Neurodegener Dis*. 2010; 7:80–83.10.1159/000285511 [PubMed: 20173332]
45. Stephens B, et al. Evidence of a breakdown of corticostriatal connections in Parkinson's disease. *Neuroscience*. 2005; 132:741–754.10.1016/j.neuroscience.2005.01.007 [PubMed: 15837135]
46. Zaja-Milatovic S, et al. Dendritic degeneration in neostriatal medium spiny neurons in Parkinson disease. *Neurology*. 2005; 64:545–547.10.1212/01.WNL.0000150591.33787.A4 [PubMed: 15699393]

47. Sulzer D. How addictive drugs disrupt presynaptic dopamine neurotransmission. *Neuron*. 2011; 69:628–649.10.1016/j.neuron.2011.02.010 [PubMed: 21338876]
48. Deng J, et al. Structure of the ROC domain from the Parkinson's disease-associated leucine-rich repeat kinase 2 reveals a dimeric GTPase. *Proceedings of the National Academy of Sciences of the United States of America*. 2008; 105:1499–1504.10.1073/pnas.0709098105 [PubMed: 18230735]
49. Watabe-Uchida M, Zhu L, Ogawa SK, Vamanrao A, Uchida N. Whole-brain mapping of direct inputs to midbrain dopamine neurons. *Neuron*. 2012; 74:858–873.10.1016/j.neuron.2012.03.017 [PubMed: 22681690]
50. Glaser EM, Van der Loos H. Analysis of thick brain sections by obverse-reverse computer microscopy: application of a new, high clarity Golgi-Nissl stain. *J Neurosci Methods*. 1981; 4:117–125. [PubMed: 6168870]
51. Gibb R, Kolb B. A method for vibratome sectioning of Golgi-Cox stained whole rat brain. *J Neurosci Methods*. 1998; 79:1–4. [PubMed: 9531453]
52. Steiner P, et al. Destabilization of the postsynaptic density by PSD-95 serine 73 phosphorylation inhibits spine growth and synaptic plasticity. *Neuron*. 2008; 60:788–802.10.1016/j.neuron.2008.10.014 [PubMed: 19081375]
53. Mathur BN, Capik NA, Alvarez VA, Lovinger DM. Serotonin induces long-term depression at corticostriatal synapses. *J Neurosci*. 2011; 31:7402–7411.10.1523/JNEUROSCI.6250-10.2011 [PubMed: 21593324]
54. Tang K, Low MJ, Grandy DK, Lovinger DM. Dopamine-dependent synaptic plasticity in striatum during in vivo development. *Proceedings of the National Academy of Sciences of the United States of America*. 2001; 98:1255–1260.10.1073/pnas.031374698 [PubMed: 11158626]
55. Cai H, et al. Loss of ALS2 function is insufficient to trigger motor neuron degeneration in knock-out mice but predisposes neurons to oxidative stress. *J Neurosci*. 2005; 25:7567–7574.10.1523/JNEUROSCI.1645-05.2005 [PubMed: 16107644]
56. Jiang M, Chen G. High Ca²⁺-phosphate transfection efficiency in low-density neuronal cultures. *Nat Protoc*. 2006; 1:695–700.10.1038/nprot.2006.86 [PubMed: 17406298]
57. Peng J, et al. Semiquantitative proteomic analysis of rat forebrain postsynaptic density fractions by mass spectrometry. *J Biol Chem*. 2004; 279:21003–21011.10.1074/jbc.M400103200 [PubMed: 15020595]
58. Chandran JS, et al. Progressive behavioral deficits in DJ-1-deficient mice are associated with normal nigrostriatal function. *Neurobiol Dis*. 2008; 29:505–514.10.1016/j.nbd.2007.11.011 [PubMed: 18187333]
59. Napolitano F, et al. Role of aberrant striatal dopamine D1 receptor/cAMP/protein kinase A/DARPP32 signaling in the paradoxical calming effect of amphetamine. *J Neurosci*. 2010; 30:11043–11056.10.1523/JNEUROSCI.1682-10.2010 [PubMed: 20720111]

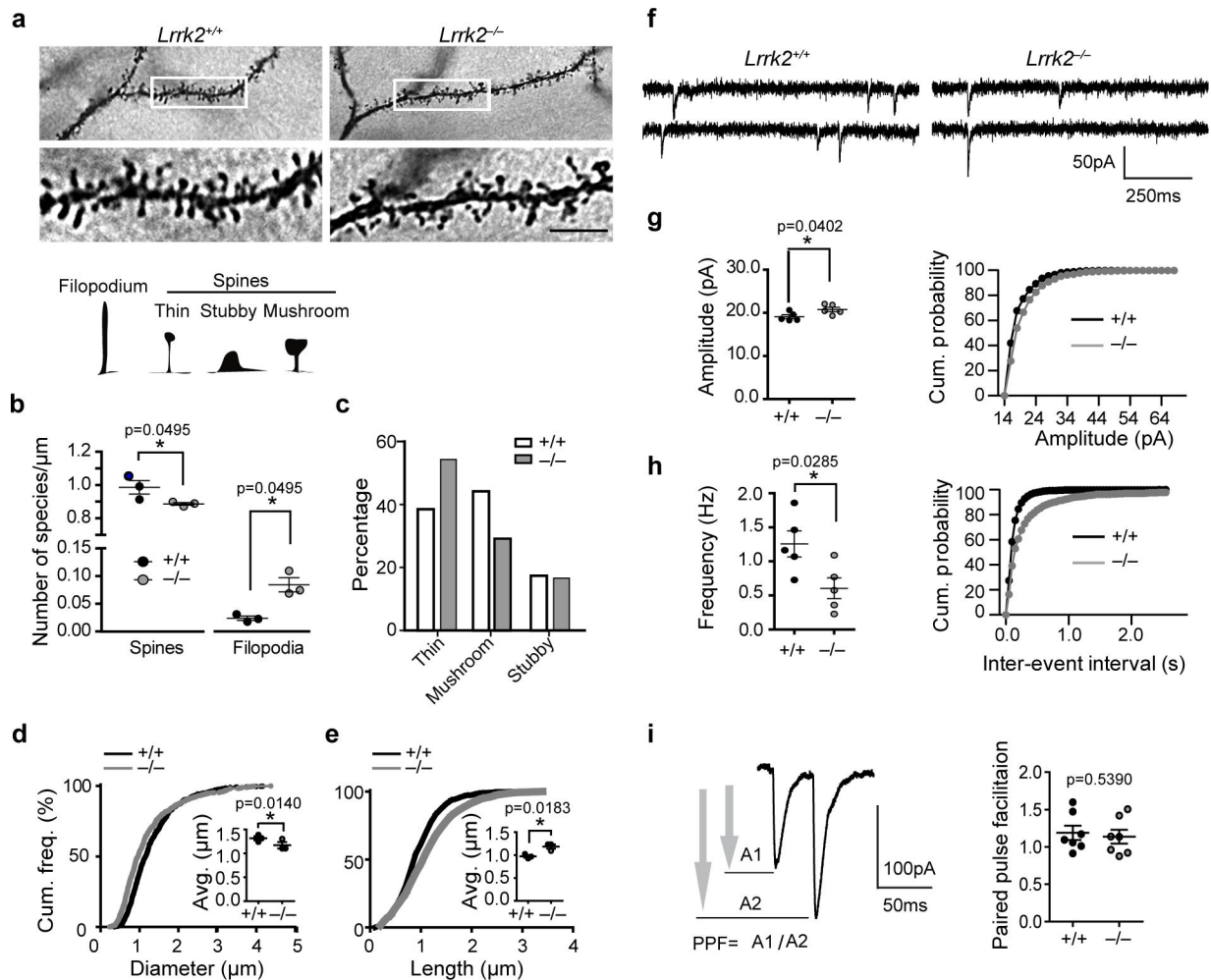


Figure 1. Loss of *LRRK2* leads to decreased number of mature spines and altered synaptic transmission

(a) Golgi-Cox staining of SPNs from P15 littermate *LRRK2*^{+/+} and *LRRK2*^{-/-} pups. The bottom panels are enlargement of boxed areas of the upper panels. Scale bar: 5 μm . (b) The density of dendritic spines and filopodia ($n=3$ three pups per genotype). Data represent mean \pm SEM. Mann-Whitney Test (spine: $z=1.964$, filopodia: $z=-1.964$). * $P<0.05$. The inset shows schematic representation of filopodium and different types of dendritic spines. (c) The distribution of different types of dendritic spines in *LRRK2*^{+/+} and *LRRK2*^{-/-} SPNs ($n_{LRRK2}^{+/+}=839$ spines, $n_{LRRK2}^{-/-}=835$ spines from six neurons of three pups per genotype, Chi-Squared test ($\chi^2_{(2)}=50.13$), $p<0.0001$). (d,e) Cumulative frequencies of spine head diameter (d, KS-test, $p<0.001$) and spine length (e, KS-test, $p<0.001$) in the spines of SPNs described above. Scatter blots show average head diameter and length. Data represent mean \pm SEM. Unpaired t-test, $t_{(4)}=1.839$ and 3.853, respectively. * $P<0.05$. (f) Traces of mEPSCs recorded from P15 *LRRK2*^{+/+} and *LRRK2*^{-/-} SPNs. (g, h) Mean values and cumulative distribution for amplitude (g, Unpaired t-test, $t_{(8)}=2.446$; KS-test, * $p<0.01$) and frequency (h, Unpaired t-test, $t_{(8)}=2.667$; KS-test, $p<0.001$) of mEPSCs from P15 pups ($n_{LRRK2}^{+/+}=11$ neurons, $n_{LRRK2}^{-/-}=13$ neurons of five pups per genotype). Data represent mean \pm

SEM. * $P < 0.05$. (i) Paired-pulse facilitation measured at a 50ms inter-pulse interval and summary data for $n_{LRRK2^{+/+}} = 5$ neurons, $n_{LRRK2^{-/-}} = 7$ neurons ($t_{(12)} = 0.6323$).

Author Manuscript

Author Manuscript

Author Manuscript

Author Manuscript

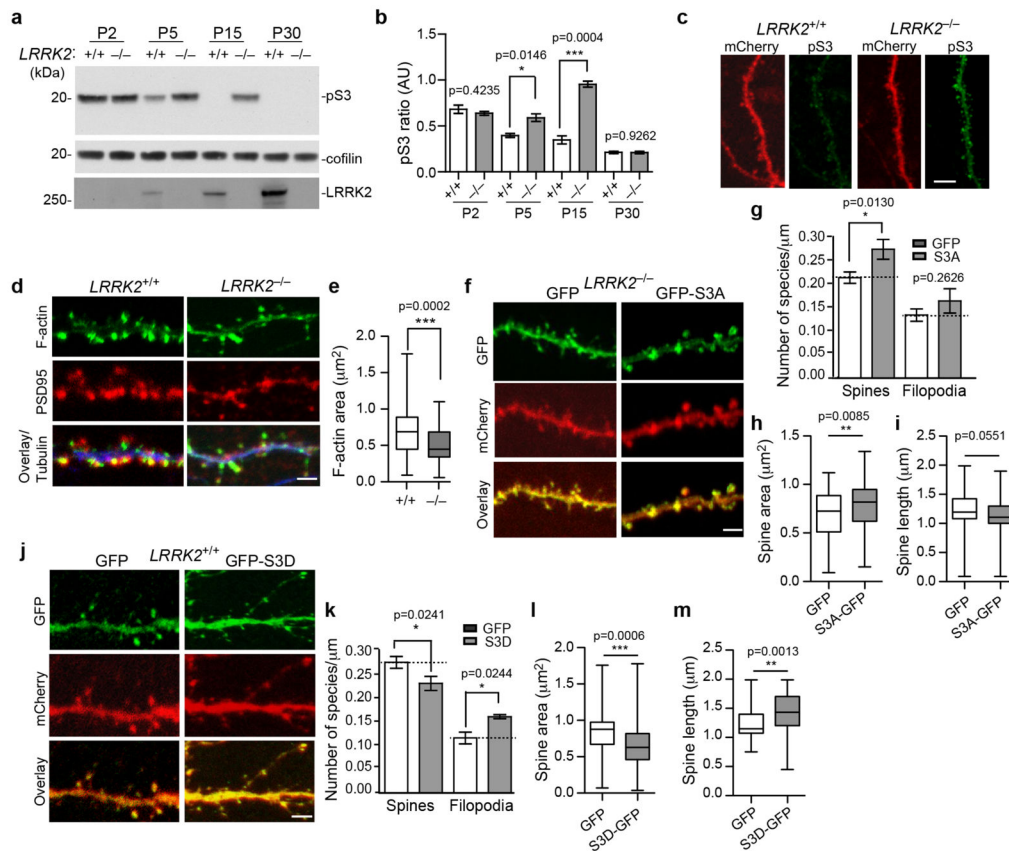


Figure 2. Abnormal phosphorylation of cofilin in $LRRK2^{-/-}$ neurons
(a) Western blot analysis of forebrain homogenates from $LRRK2^{+/+}$ and $LRRK2^{-/-}$ mice. The full-length images are shown in Supplementary Fig. 2e. **(b)** The pS3 cofilin levels normalized against total cofilin levels ($n=3$ per genotype). Data represent mean \pm SEM, Unpaired t-test, $t_{(4)}=0.8906, 0.1047, 11.11, \text{ and } 4.117$, respectively. * $p<0.05$, *** $p<0.001$. **(c)** Representative images of spines and their parental dendrites of cultured $LRRK2^{+/+}$ and $LRRK2^{-/-}$ hippocampal neurons transfected with mCherry (red) and stained with pS3 cofilin (green). Scale bar: $10\mu\text{m}$. **(d)** Staining of F-actin (green), PSD95 (red), and β III-tubulin (blue) in dendritic spines and corresponding dendrites of $LRRK2^{+/+}$ and $LRRK2^{-/-}$ hippocampal neurons at 15DIV. Scale bar: $5\mu\text{m}$. **(e)** F-actin area staining in the dendritic spine of $LRRK2^{+/+}$ and $LRRK2^{-/-}$ hippocampal neurons ($n=6-8$ neurons per genotype; $n=85-90$ spines per genotype). Data represent mean \pm SEM. Unpaired t-test, *** $p<0.001$. **(f, j)** Spines and dendritic regions of $LRRK2^{-/-}$ **(f)** and $LRRK2^{+/+}$ **(j)** hippocampal neurons transfected with GFP, GFP-S3A, and GFP-S3D cofilin plasmids, along with mCherry at 15DIV. Scale bar: $5\mu\text{m}$. **(g, k)** Density of dendritic spines and filopodia was quantified from $LRRK2^{-/-}$ and $LRRK2^{+/+}$ neurons. **(h-i, l-m)** Bar graphs showing average head spine diameter and dendritic spine length of transfected $LRRK2^{-/-}$ **(h, i)** and $LRRK2^{+/+}$ neurons **(l, m)** ($LRRK2^{-/-}$, $n_{\text{GFP}}=73$ spines, $n_{\text{S3A-GFP}}=80$ spines; $LRRK2^{+/+}$, $n_{\text{GFP}}=101$ spines, $n_{\text{S3D-GFP}}=79$ spines; Four to seven neurons per genotype). Data represent mean \pm SEM. Unpaired t-test, * $p<0.05$, ** $p<0.01$, *** $p<0.001$

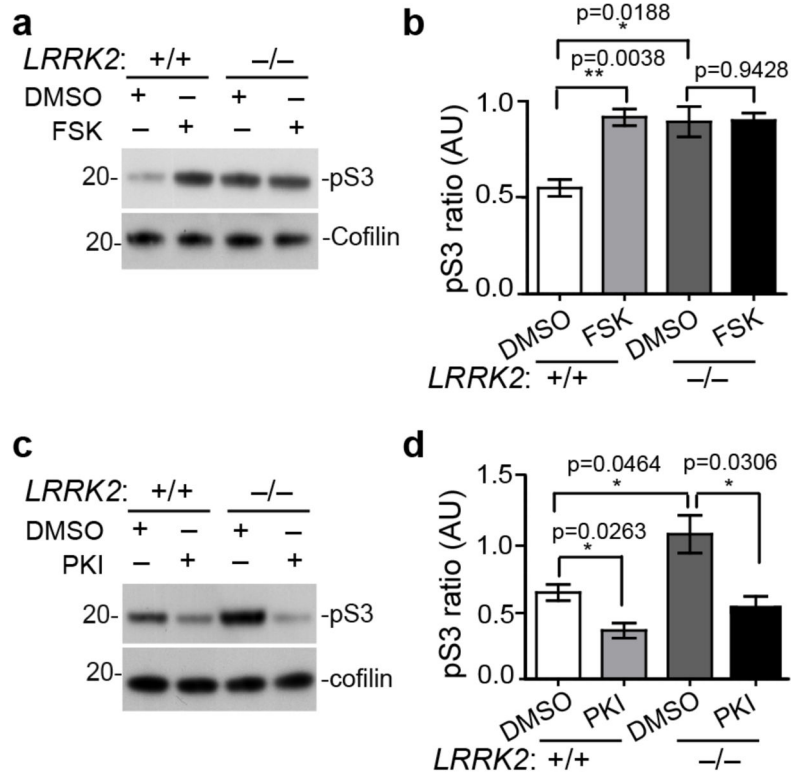


Figure 3. PKA signaling is involved in *LRRK2*-dependent phosphorylation of cofilin
(a, b) Western Blot analysis of cultured *LRRK2*^{+/+} and *LRRK2*^{-/-} cortical neurons treated with DMSO or FSK (50μM for 1 hr) and **(c, d)** DMSO or PKI (5μM for 24 hrs) for the expression of phosphorylated and total cofilin. Three or more independent cultures were analyzed per genotype and per treatment. Data represent mean ± SEM. Unpaired t-test, $t_{(4)}=6.019, 3.820, \text{ and } 0.0764$, respectively in **(b)**. $t_{(4)}=3.441, 2.851, \text{ and } 3.278$, respectively in **(d)**. * $P<0.05$, ** $p<0.01$. The full-length images in Fig. 3a and 3c are shown in Supplementary Fig. 3m and 3n.

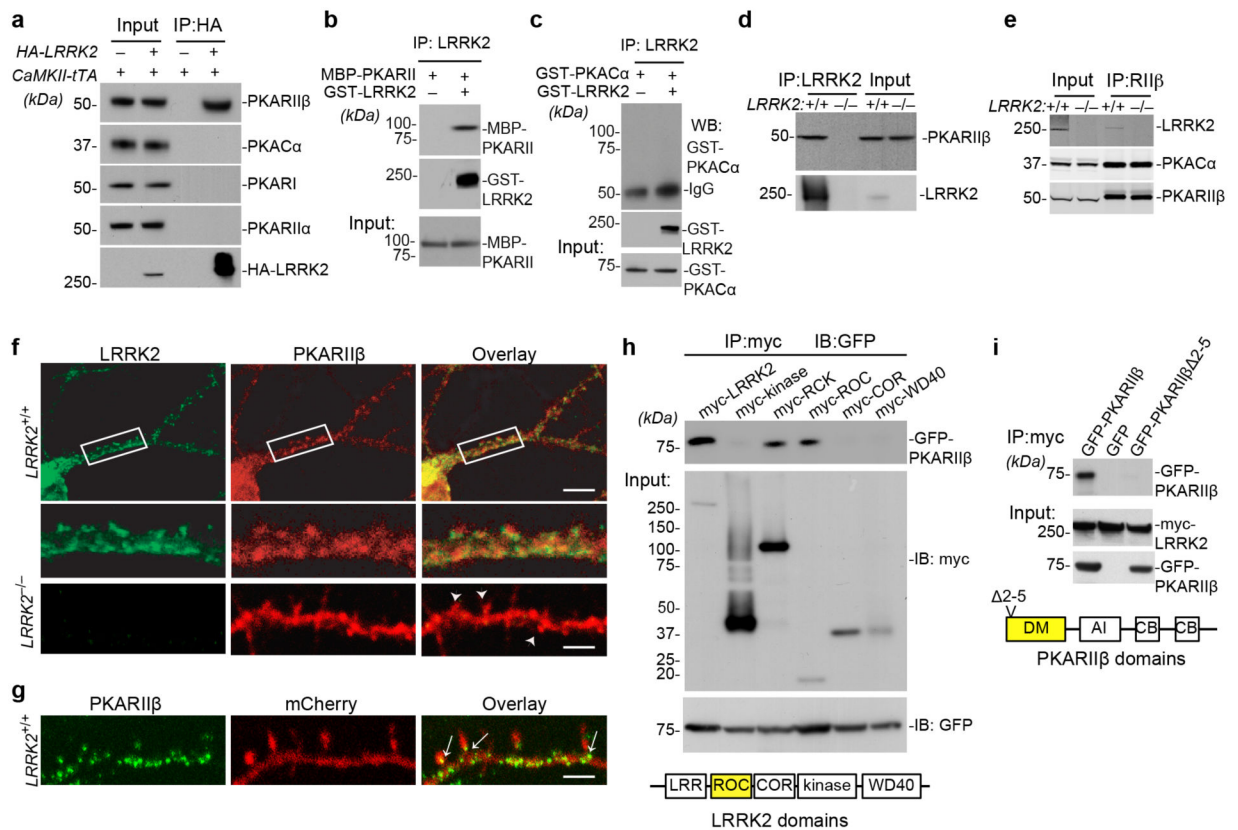


Figure 4. LRRK2 interacts with PKARII β

(a) Co-IP of transgenic human wild-type LRRK2 and endogenous mouse PKARII β from the forebrain homogenate of P15 *CaMKII-tTA/tetO-LRRK2* double and littermate *CaMKII-tTA* single transgenic mice. The N-terminal of transgenic LRRK2 is HA-tagged. (b,c) Co-IP of GST-tagged recombinant human LRRK2 proteins with maltose-binding protein (MBP)-tagged recombinant mouse PKARII β proteins (b) and GST-tagged recombinant mouse PKAC α proteins (c). (d) Co-IP of endogenous mouse LRRK2 and PKARII β from the light membrane fractions of P15 mouse striatal tissues. (e) Co-IP of endogenous mouse LRRK2, PKAC α and PKARII β from the light membrane fractions of P15 mouse striatal tissues using a PKARII β antibody. (f) Co-staining of endogenous LRRK2 (green) and PKARII β (red) in cultured mouse hippocampal neurons at 15DIV. The middle two panels show the boxed areas in the top panel. The bottom panel shows LRRK2 (green) and PKARII β (red) staining in 15DIV *LRRK2*^{-/-} hippocampal neurons (arrowheads point to dendritic spines). Scale bars: 20 μ m (top panel), 5 μ m (lower panels). (g) Representative image shows subcellular localization of endogenous PKARII β (green) in the dendrite of mCherry-transfected 15DIV *LRRK2*^{+/+} hippocampal neurons. Arrowheads indicate the localization of PKARII β at the base of dendritic spines. Scale bars: 5 μ m. (h) Co-IP of GFP-PKARII β with myc-tagged human wild-type full-length LRRK2, as well as LRRK2 kinase, RCK (Roc-COR-Kinase), ROC, COR, and WD40 domains from transfected HEK293 cells. (i) Co-IP of myc-tagged human wild-type full-length LRRK2 with GFP, GFP-PKARII β , and GFP-PKARII β 2–5 from transfected HEK293 cells. DM: dimerization domain, AI: auto-inhibitory domain, CB:

cAMP binding domain. The full-length images in Fig. 4a–e, 4h, and 4j are shown in Supplementary Fig. 4g–k, 4l, and 4m.

Author Manuscript

Author Manuscript

Author Manuscript

Author Manuscript

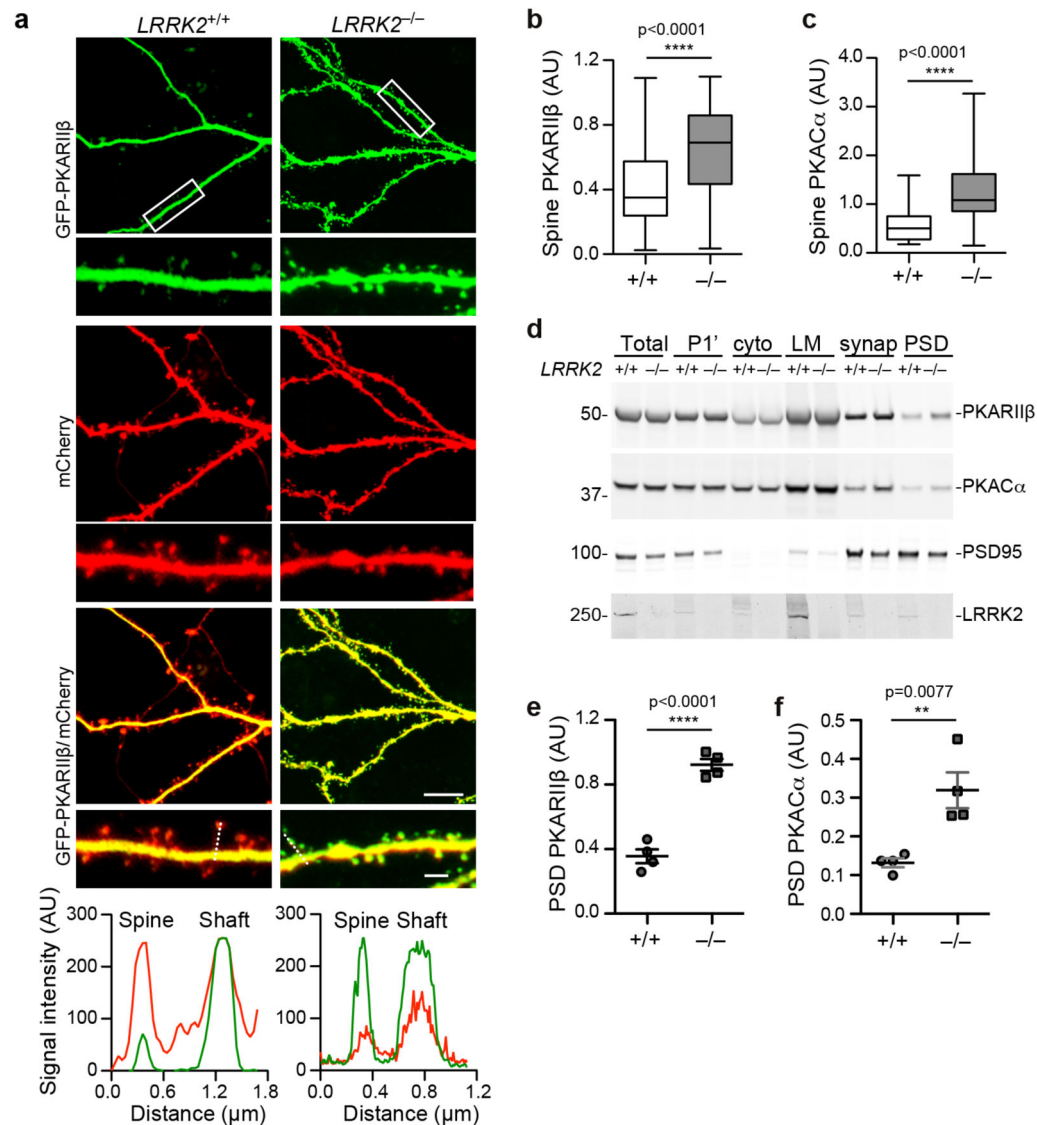


Figure 5. LRRK2 regulates the subcellular localization of PKARIIβ

(a) Fluorescent images of GFP-PKARIIβ and mCherry in dendrites of transfected *LRRK2*^{+/+} and *LRRK2*^{-/-} hippocampal neurons at 15DIV. Scale bars: 5μm (lower magnification), 1μm (higher magnification). The RGB signal profile shows mCherry (red) and GFP-PKARIIβ (green) expression across the spine and adjacent dendritic shaft section depicted by the discontinuous white line on *LRRK2*^{+/+} and *LRRK2*^{-/-} hippocampal neurons. (b,c) The relative ratio of GFP-PKARIIβ (b) and GFP-PKACα (c) in the dendritic spine versus adjacent dendritic shaft of *LRRK2*^{+/+} and *LRRK2*^{-/-} hippocampal neurons at 15DIV ($n=52-95$ spines of seven neurons per genotype). Data represent mean \pm SEM. Unpaired t-test, $t_{(114)}=7.013$ in (c). *** $p < 0.001$, **** $p < 0.0001$. (d) Western blot analysis of endogenous PKARIIβ, PKACα, PSD95, and LRRK2 expression in the total, pelleted nuclear and other insoluble (P1'), cytosol, light membrane (LM), synaptosome (synap) and PSD fractions of P15 *LRRK2*^{+/+} and *LRRK2*^{-/-} mouse brain homogenates. The full-length images are shown in Supplementary Fig. 5e. (e,f) Quantified data of PKARIIβ (e) and PKACα (f) protein

levels in the PSD fraction of P15 *LRRK2*^{+/+} and *LRRK2*^{-/-} mouse brain homogenates (*n*=4 per genotype). Data represent mean ± SEM. Unpaired t-test, $t_{(6)}=9.929$ and 3.935, respectively. ** $P<0.01$, **** $p<0.0001$.

Author Manuscript

Author Manuscript

Author Manuscript

Author Manuscript

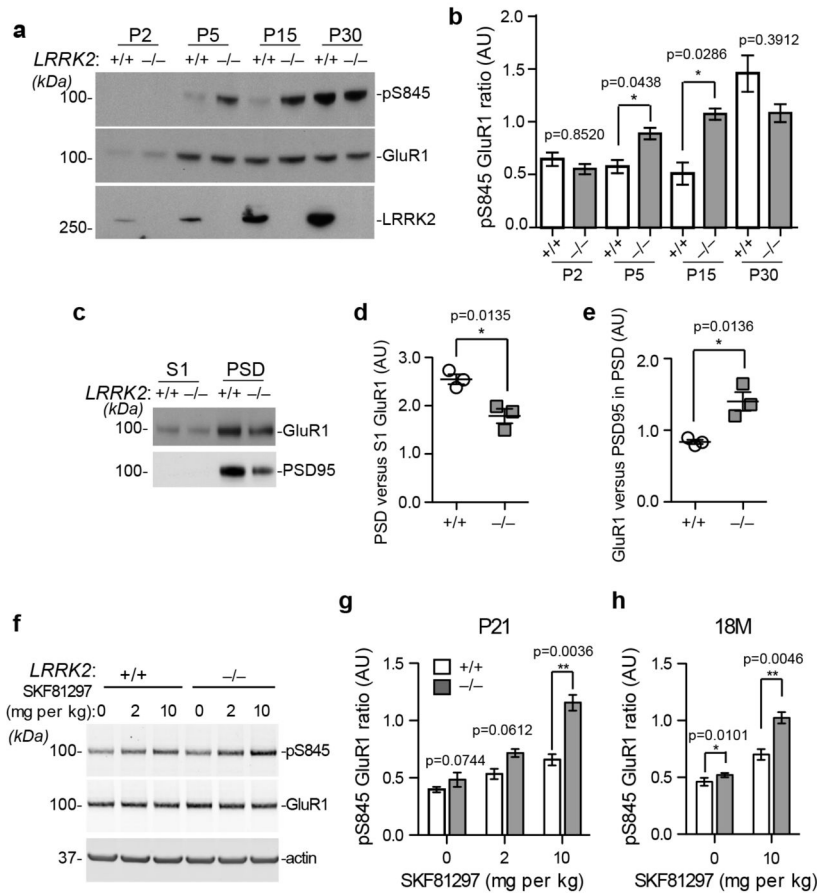


Figure 6. Loss of *LRRK2* causes alteration of PKA-dependent phosphorylation of GluR1 in young and aged mice

(a) Western blot analysis of pS845 GluR1, total GluR1 and LRRK2 expression in the forebrain homogenates of P2, P5, P15, and P30 *LRRK2*^{+/+} and *LRRK2*^{-/-} mice. (b) Quantification analysis of pS845 GluR1 levels normalized to total GluR1 levels derived of three independent experiments. Data represent mean \pm SEM. Unpaired t-test, $t_{(4)}=0.5791$, 6.282, 3.576, and 1.061, respectively. * $p<0.05$, ** $p<0.01$. (c) Western blot analysis of GluR1 and PSD95 in the S1 and PSD fractions of P15 *LRRK2*^{+/+} and *LRRK2*^{-/-} mouse brains. (d,e) Quantification analysis of GluR1 levels in the PSD versus S1 fractions of brain extracts (d), as well as GluR1 levels versus PSD95 levels in the PSD fraction of brain extracts (e). $n=3$ per genotype. Data represent mean \pm SEM. Unpaired t-test, $t_{(4)}=4.218$ (d) and 4.206 (e). * $p<0.05$. (f) Western blot analysis of pS845 and total GluR1 in the striatum of P21 *LRRK2*^{+/+} and *LRRK2*^{-/-} mice after treated with saline (0) or Drd1 agonist SKF81297 at 2 and 10mg per kg bodyweight. Actin was used as the loading control. (g,h) Quantification analysis of pS845 GluR1 ratio in the striatal tissues of P21 (g) and 18-month-old mice (h) treated with SKF81297. $n=4$ per genotype per treatment. Data represent mean \pm SEM. Unpaired t-test. $t_{(8)}=2.501$, 2.177, and 4.605 in (g). $t_{(6)}=3.703$ and 4.401 in (h). * $p<0.05$, ** $p<0.01$. The full-length images of Fig. 6a,c,f are shown in Supplementary Fig. 6h-j.

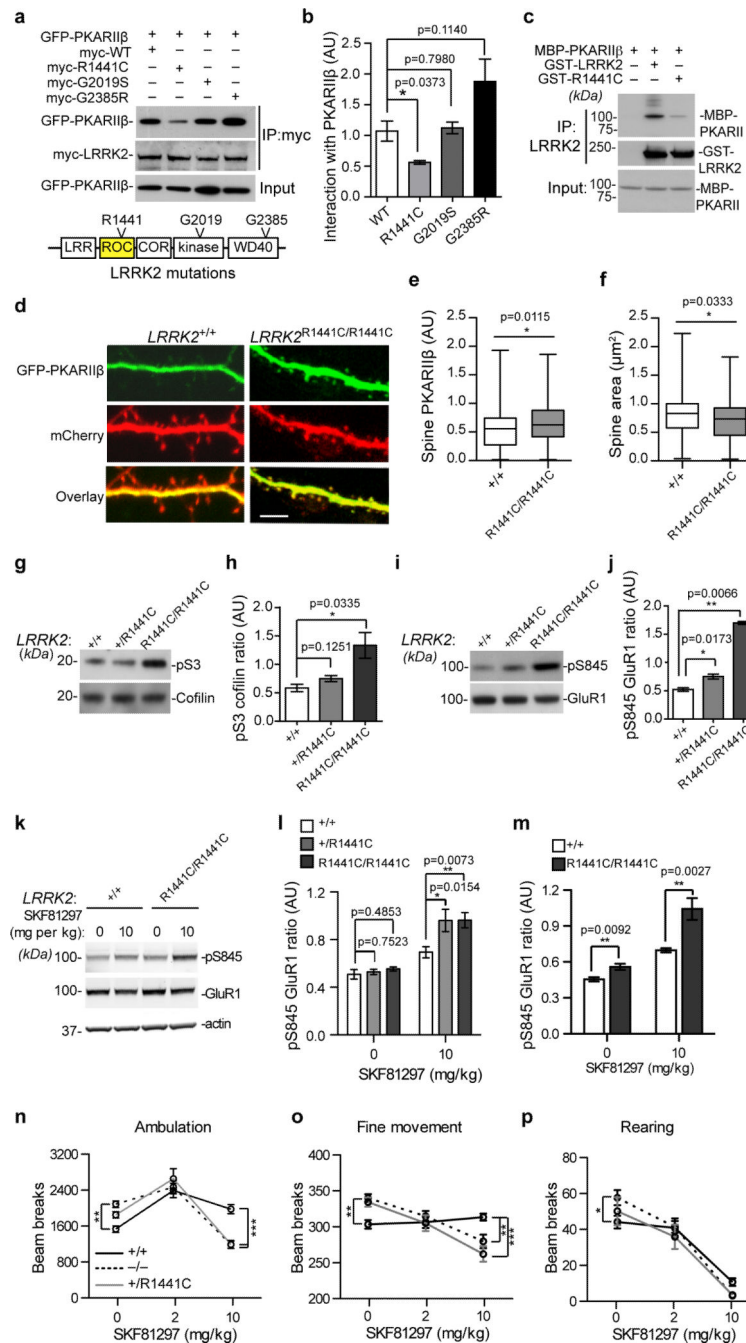


Figure 7. The R1441C mutation impairs the regulatory function of LRRK2 on PKA
 (a) Co-IP of GFP-PKARIIB with wild-type, R1441C, G2019S, and G2385 LRRK2 from transfected cells (a). (b) The relative binding affinity of GFP-PKARIIB with LRRK2 proteins ($n=3$). $t_{(4)}=3.070$, 0.2735 , and 2.016 . (c) Co-IP of GST-LRRK2 and GST-R1441C with MBP-PKARIIB recombinant proteins. (d) GFP-PKARIIB and mCherry signals in the spines and dendrites of 15DIV cultured hippocampal neurons. Scale bar: $5\mu\text{m}$. (e,f) Quantification of GFP-PKARIIB signal in the spines (f, $n=70-75$ spines from six neurons per genotype), and the spine size (g, $n=60$ spines from four neurons per genotype). $t=2.552$

and 2,145, respectively. **(h-k)** The pS3 versus total cofilin **(h,i)** and pS845 versus total GluR1 **(j,k)** in the forebrain homogenate of P15 *LRRK2*^{+/+}, *LRRK2*^{+/^{R1441C}} and *LRRK2*^{R1441C/R1441C} mice. *n*=3 per genotype. *t*₍₄₎=1.935 and 3.182 in **(h)**, 3.918 and 5.191 in **(j)**. **(l-n)** The pS845 versus total GluR1 in the striatum of P21 *LRRK2*^{+/+} (*n*=8), *LRRK2*^{+/^{R1441C}} (*n*=4), and *LRRK2*^{R1441C/R1441C} (*n*=4) mice **(l,m)**, and 18-month-old *LRRK2*^{+/+} (*n*=4) and *LRRK2*^{RC/RC} (*n*=4) mice **(n)**. *t*₍₁₀₎=0.3237, 0.7222, 2.865, and 3.283 in **(m)**. *t*₍₆₎=3.303 and 4.083 in **(m)**. **(o-q)** The ambulatory **(o)**, fine **(p)**, and rearing movement **(q)** of P21 *LRRK2*^{+/+}, *LRRK2*^{-/-}, and *LRRK2*^{+/^{RC}} mice after treated with saline (*n*=16, 37, and 10) or SKF81297 at 2 (*n*=21, 28, and 11) and 10mg per kg bodyweight (*n*=27, 28, and 10). Data represent mean ± SEM. Unpaired test **(b,e,f,h,j,l,m)** and two-way ANOVA plus Bonferroni post-tests **(m-q)** were used.

Author Manuscript

Author Manuscript

Author Manuscript

Author Manuscript